ESC European Society of Cardiology

Cardiovascular Research (2018) **114**, 1029–1040
doi:10.1093/cvr/cvy067

Sustained release of endothelial progenitor cell-derived extracellular vesicles from shear-thinning hydrogels improves angiogenesis and promotes function after myocardial infarction

Carol W. Chen[1], Leo L. Wang[2], Samir Zaman[1], Jon Gordon[1], Maria F. Arisi[1], Chantel M. Venkataraman[1], Jennifer J. Chung[1], George Hung[1], Ann C. Gaffey[1], Lynn A. Spruce[3], Hossein Fazelinia[3], Robert C. Gorman[1], Steven H. Seeholzer[3], Jason A. Burdick[2], and Pavan Atluri[1]*

[1]Division of Cardiovascular Surgery, Department of Surgery, University of Pennsylvania, Silverstein 6, 3400 Spruce Street, Philadelphia, PA 19104, USA; and [2]Department of Bioengineering, University of Pennsylvania, 240 Skirkanich, 210 S 33rd Street, Philadelphia, PA 19104; and [3]Protein and Proteomics Core Facility, The Children's Hospital of Philadelphia Research Institute, 3615 Civic Center Boulevard, Philadelphia, PA 19104, USA

Received 28 February 2017; revised 12 August 2017; editorial decision 30 October 2017; accepted 15 March 2018; online publish-ahead-of-print 16 March 2018

Time for primary review: 40 days

Aims Previous studies have demonstrated improved cardiac function following myocardial infarction (MI) after administration of endothelial progenitor cells (EPCs) into ischaemic myocardium. A growing body of literature supports paracrine effectors, including extracellular vesicles (EVs), as the main mediators of the therapeutic benefits of EPCs. The direct use of paracrine factors is an attractive strategy that harnesses the effects of cell therapy without concerns of cell engraftment or viability. We aim to reproduce the beneficial effects of EPC treatment through delivery of EPC-derived EVs within a shear-thinning gel (STG) for precise localization and sustained delivery.

Methods and results EVs were harvested from EPCs isolated from adult male *Rattus norvegicus* (Wistar) rats and characterized by electron microscopy, nanoparticle tracking analysis (NTA), and mass spectrometry. EVs were incorporated into the STG and injected at the border zone in rat models of MI. Haemodynamic function, angiogenesis, and myocardial remodelling were analyzed in five groups: phosphate buffered saline (PBS) control, STG control, EVs in PBS, EVs in STG, and EPCs in STG. Electron microscopy and NTA of EVs showed uniform particles of 50–200 nm. EV content analysis revealed several key angiogenic mediators. EV uptake by endothelial cells was confirmed and followed by robust therapeutic angiogenesis. *In vivo* animal experiments demonstrated that delivery of EVs within the STG resulted in increased peri-infarct vascular proliferation, preservation of ventricular geometry, and improved haemodynamic function post-MI.

Conclusions EPC-derived EVs delivered into ischaemic myocardium via an injectable hydrogel enhanced peri-infarct angiogenesis and myocardial haemodynamics in a rat model of MI. The STG greatly increased therapeutic efficiency and efficacy of EV-mediated myocardial preservation.

Keywords Endothelial progenitor cells • Extracellular vesicles • Exosomes • Hydrogel • Angiogenesis

1. Introduction

Heart disease is the leading cause of death for Americans with ~720,000 people experiencing a heart attack every year.[1] Despite advances in reperfusion therapy, incomplete myocardial revascularization remains as high as 37% after coronary artery bypass grafting and 43% after percutaneous coronary intervention.[2] After an ischaemic event, myocyte necrosis and subsequent alteration of the loading pattern activate a cascade of neurohormonal signalling that mediates cardiac remodelling through ventricular dilatation, hypertrophy, and the formation of a

* Corresponding author. Tel: +1 215 662 2956; fax: +1 215 349 5798, E-mail: pavan.atluri@uphs.upenn.edu

collagen scar. Though this remodelling may temporarily preserve cardiac output, progressive remodelling is maladaptive and leads to further ventricular dilatation and potentially heart failure.[3]

Therapeutic angiogenesis is a potential strategy to foster new vessel formation in the ischaemic peri-infarct border zone and to subsequently improve post-infarction ventricular remodelling and cardiac function. However, studies investigating the direct injection of progenitor cells into the myocardium to improve local angiogenesis have struggled with low cell retention and viability.[4,5] Nevertheless, recent studies have demonstrated the persistence of the therapeutic effect of myocardially transplanted cells in the absence of cell engraftment, suggesting the potential for paracrine mechanisms derived from the cell secretome as the therapeutic mediators.[6,7] Extracellular vesicles (EVs), including exosomes and microvesicles, have garnered significant interest due to their key roles in paracrine signalling with angiogenic, proliferative, and anti-apoptotic effects.[8,9]

Exosomes are nanovesicles with characteristic size of 40–120 nm formed by the budding of the endosomal membrane into a multivesicular body created by the inward invagination of the lipid bilayer plasma membrane. In contrast, microvesicles range from 50 to 1000 nm and are formed by the outward budding of the plasma membrane resulting in vesicular membranes that closely resemble that of the cell.[10] Though exosomes are more uniform in size and protein content, significant overlap in function exists between exosomes and microvesicles. A wide range of signalling molecules including proteins, mRNA, and miRNA, are transported within exosomes and microvesicles to mediate cross-talk between cells.[11,12] The potential for replicating the angiogenic activity of progenitor cells using EVs alone while eliminating the complexities associated with cell transplantation and survival is a very attractive strategy. We hypothesize that this cell-free therapy will confer several distinct advantages over current cell therapies. Unlike cells, EVs can be produced and isolated in large quantities, frozen indefinitely, thawed, and rapidly prepared for therapeutic use.[13]

We postulate that EVs exert their effect on endothelial and myocardial cells over time. Given previous cell-based studies and the small size of EVs, an unacceptably high rate of washout from the myocardium is likely with direct injection. We therefore propose the use of a shear-thinning, injectable hyaluronic acid (HA) hydrogel to localize the EVs to the ischaemic border zone through encapsulation within the hydrogel. Our shear-thinning hydrogel (STG) is assembled by guest-host interactions of adamantane-modified HA (Ad-HA) and β-cyclodextrin-modified HA (CD-HA). With the application of shear stress during injection through a syringe, the construct enters a liquid-like state to allow for intramyocardial delivery. It rapidly self-heals at the target site into gel form with removal of shear stress. Through diffusion, swelling, and gel erosion, particle release is achieved over prolonged therapeutic timeframes. These properties permit slow elution of EVs and achieve high local concentrations in the ischaemic border zone.

Our group previously demonstrated that the addition of a STG to endothelial progenitor cell (EPC) treatment further augmented the improvement in cardiac function after myocardial infarction (MI) seen with injection of EPCs alone.[14] The goal of this project is to deliver EPC-derived EVs into ischaemic myocardium within a STG to reproduce the benefits of the EPC treatment in a cell-free manner. We hypothesized that delivery of EVs will increase angiogenic activity and provide peri-infarct stabilization, thereby decreasing adverse ventricular remodelling and subsequent loss of cardiac function. The primary endpoint of the study is preload-independent myocardial contractility [end systolic pressure–volume relationship (ESPVR)] measured 4 weeks after left anterior descending coronary artery (LAD) ligation and treatment. Secondary endpoints are *in vivo* angiogenesis and myocardial scar thickness.

2. Methods

2.1 Phase I. EV characterization

2.1.1 Animal use

All experiments conformed to the National Institute of Health Guide for Care and Use of Laboratory Animals and were approved by the Institutional Animal Care and Use Committee of the University of Pennsylvania. Male *Rattus norvegicus* (Wistar) rats were obtained from Charles River Laboratories, Inc (Boston, MA).

2.1.2 Cell culture

Pooled human umbilical vein endothelial cells (HUVECs) were purchased from Lonza. HUVECs were cultured in EGM-2 and passaged at 70–80% confluence up until Passage 7.

Primary bone marrow-derived rat EPCs were isolated as previously described.[14,15] Briefly, adult donor rats (350–375 g) were administered pentobarbital via intraperitoneal injection at 100 mg/kg for anaesthesia. After cessation of pedal reflex, euthanasia was performed by transection of the carotid artery, and pneumothorax was induced for confirmation of euthanasia. Following exsanguination, the long bones were collected, and the bone marrow was harvested. Bone marrow mononuclear cells were isolated by density-gradient centrifugation on Histopaque-1083 (Sigma-Aldrich, 10831) and plated on vitronectin-coated 10-cm culture dishes. EPCs were cultured as the adherent fraction in EGM-2 (Lonza, Basel, Switzerland) without heparin or hydrocortisone. After 4 days, media was changed to remove non-adherent cells. All EPCs were used 6–7 days post-isolation.

All cells were cultured at 37°C in a humidified incubator with 21% O_2 and 5% CO_2.

2.1.3 Isolation of EVs

Four days post-isolation, EPCs were changed to serum-free EGM-2 without heparin or hydrocortisone for 48 h. This conditioned media (CM) was cleared of cellular debris and large subcellular contaminants by centrifugation at 2000*g* for 30 min. EVs were isolated from clarified CM using Total Exosome Isolation reagent (Invitrogen, Carlsbad, CA) following manufacturer's protocol. Briefly, CM was incubated in a 1:2 ratio with the reagent overnight at 4°C, then pelleted by centrifugation at 10 000*g* in 4°C for 1 h and re-suspended in 0.22 μm-filtered dPBS. EPC survival after 48 h of culture in serum-free media was quantified (see Supplementary Material online).

2.1.4 Transmission electron microscopy

EV samples fixed in 2% PFA overnight were adhered to a freshly glow-discharged carbon-formvar coated 400-mesh copper grid for 20 min. Grids were negative-stained with two drops of 2% uranyl acetate for 5 min and allowed to air dry. EV preparations were analyzed by transmission electron microscopy (TEM) using a JEOL 1010 (JEOL, Ltd., Tokyo, Japan). Images were acquired using a Hamamatsu digital camera using the AMT Advantage Image Capture Software. Particle size was analyzed using ImageJ software (NIH, Bethesda, MD).

2.1.5 Nanoparticle tracking analysis

EVs suspended in phosphate buffered saline (PBS) were analyzed using the NanoSight NS500 with green laser at 532 nm (Malvern Instruments, Malvern, UK). Samples were injected manually, and data acquisition was performed at ambient temperature. Data were analyzed with Nanoparticle Tracking Analysis software (NTA 2.2; Malvern).

2.1.6 Mass spectrometry

Protein content of EPCs from cell lysate and EPC-derived EVs was prepared and analyzed by mass spectrometry using MaxQuant version 1.5.1.2 (Max Planck Institute of Biochemistry, Munich, Germany) (see Supplementary Material onlie).

2.1.7 Cellular uptake of fluorescently labelled EVs

Isolated EVs were labelled with Celltracker CM-DiI (Thermo Fisher Scientific), a strongly fluorescent lipophilic stain. EVs re-suspended in 0.22 μm-filtered Dulbecco's phosphate-buffered saline (dPBS) were incubated with 2 μM CM-DiI for 5 min at 37°C, then 15 min at 4°C. Unincorporated stain was removed using Exosome Spin Columns (Thermo Fisher Scientific) according to manufacturer's protocol. For qualitative EV uptake blocking experiments, HUVECs seeded at 1.5×10^4 cells per well on an 8-well chamber slide were pre-incubated with 0.5, 1, and 5 μM of cytochalasin D (CytoD; Sigma-Aldrich) for 30 min at 37°C. After 24 h of incubation with 4.6×10^9 CM-DiI EVs, HUVECs were fixed in 4% PFA, then stained with 5 μg/ml wheat germ agglutinin (WGA) AF-647 conjugate (Thermo Fisher Scientific) for 15 min at room temperature to visualize the cell membrane and counterstained with 4',6-diamidino-2-phenylindole (DAPI). Imaging was performed at 63× magnification on a LSM 710 (Zeiss, OberKochen, Germany) confocal microscope. Quantitative EV uptake blocking experiments were performed using the Synergy 2 Microplate Reader (BioTek, Winooski, VT) (see Supplementary Material online).

2.1.8 Tubule formation assay

The angiogenic effect of EVs on HUVECs was quantified using a Matrigel tubule formation assay. Matrigel solution (Corning, Cat no. 354234) was thawed overnight, and 225 μl was plated per well onto a 24-well plate. After a 30-min gelation period at 37°C, 7×10^4 HUVECs were seeded onto each well. HUVECs were incubated with endothelial cell basal media (EBM-2, Lonza) alone, 1 ng/ml vascular endothelial growth factor (VEGF, Sigma), or 4.6×10^9 EVs. After 11 h, the proliferative response of HUVECs to EVs was quantified (see Supplementary Material online). Bright-field micrographs at 4× were obtained using the EVOS XL Imaging System (Invitrogen). The mean tubule lengths, defined as the length between two nodes, were analyzed using the measuring tool on ImageJ. The number of isolated segments was analyzed the Angiogenesis Analyzer plug-in (Gilles Carpentier).

2.1.9 STG preparation and EV release profile

The formation of the STG was performed as described previously in[14] (see Supplementary Material online). Briefly, hydrogels at 4% w/w were prepared from lyophilized polymers of Ad-HA and CD-HA dissolved in PBS and mixed. The mechanical properties and viscoelastic behaviour of the STG were characterized with an AR2000 stress-controlled rheometer (TA Instruments, New Castle, DE). Encapsulation of EPCs or EVs was performed by dissolving the polymers in PBS suspensions of EPCs or EVs. To assess the time course of EV release, 500 μl of PBS was added on top of gels and incubated at 37°C. On Days 4, 7, 14, and 21, releasates were collected without disturbing the gel and replaced with fresh PBS. Releasates were stored at -20°C and analyzed with NTA to determine particle release.

2.2 Phase II. EV treatment

2.2.1 Rat model of MI

MI was induced by occlusion of the LAD, which is an established model of MI.[15] Animals were randomized into 1 of 5 treatment groups: PBS control ($n = 10$), STG control ($n = 10$), EVs in PBS (PBS + EV, $n = 9$), EPCs in STG (STG + EPC, $n = 10$), and EVs in STG (STG + EV, $n = 11$). EPCs or EVs prepared in STG were formed as described and manually transferred to a 1 mL syringe. Animals were induced with 5% isoflurane in an induction chamber, then intubated and mechanically ventilated, with 1–3% isoflurane to maintain a surgical anaesthetic depth for the duration of the procedure. Prior to incision, 0.05 mg/kg of buprenorphine was injected subcutaneously. The chest was entered through a left fourth interspace thoracotomy. The LAD was identified and ligated 1 mm below the level of the left atrial appendage with a resultant anterolateral MI encompassing 30% of the left ventricle (LV). Immediately after infarction, 100 μl of PBS or STG containing 700 000 EPCs or 9.33×10^9 EVs was delivered via 5×20 μl injections around the border zone of the infarcted area. During closure, 1 mg/kg of bupivacaine was injected at the intercostal incision, and meloxicam at 2 mg/kg was injected subcutaneously. Following closure, pneumothorax was evacuated. Animals were recovered on a heating pad and ventilated on room air until spontaneously breathing. For the *in vivo* studies, the EPCs and EVs were allogenic and pooled from multiple donors. The EVs injected in the STG + EV experiment group were derived from the EPCs that were injected in the STG + EPC group.

2.2.2 Measurement of haemodynamics

Four weeks following LAD ligation and treatment injection, haemodynamics were assessed. After induction of anaesthesia with 5% isoflurane, the rat was intubated and mechanically ventilated. Following confirmation of adequate surgical anaesthesia maintained with continuous inhaled 2% isoflurane, a 2Fr pressure–volume catheter (Millar, Inc., Houston, TX) was inserted into the LV in a retrograde fashion via the right common carotid artery. The primary measure of treatment effect in this study was preload-independent contractility as measured by ESPVR, which was determined by temporary occlusion of the inferior vena cava using the methods described by Pacher *et al.*[16] Additional haemodynamic parameters measured were ejection fraction, cardiac output, the rate of pressure rise in systole (+dP/dt), the rate of ventricular relaxation in diastole (-dP/dt), maximum pressure, end diastolic, end systolic, and stroke volumes, end diastolic pressure–volume relationship (EDPVR), and heart rate.

2.2.3 Immunohistochemical analysis

To assess angiogenesis in the infarct border zone, 10 μm sections taken at the mid-papillary level were stained with conjugated antibodies against Von Willebrand factor (vWF-FITC, ab8822, 1:300) and smooth muscle actin (SMA-AF594, ab202368, 1:300), and WGA-AF647 conjugate (1:300). Images were taken on the Leica DM5000b (Leica, Wetzlar, Germany) at 20× magnification using a DFC350 FX monochrome camera (Leica). Three high-power fields (HPFs) per animal were taken of the peri-infarct myocardium, defined as one field away from WGA-labelled scar. Each image was manually quantified for total vasculature using ImageJ: areas expressing vWF alone were counted as capillaries, while areas co-expressing vWF and SMA were counted as arterioles. In

addition, inflammatory cell infiltration into the peri-infarct border zone was assessed 2 days and 4 weeks after MI and treatment by staining for CD11b (see Supplementary Material online).

2.2.4 Histological analysis

At time of terminal surgery, the hearts were explanted and embedded in OCT (Tissue Tek, Torrance, CA) and frozen on dry-ice. 10 μm transverse sections were taken from the apex to the base of the LV. Sections were stained using Masson's Trichrome (Sigma-Aldrich). Scar thickness, a measure of border zone treatment response, was determined by averaging the distance between the endocardial and epicardium at the scar midpoint and at both ends of the scar on sections taken at the mid-papillary level. All measurements were made using ImageJ. Representative images were taken at the apical, middle, and basal portions of the infarct and imaged using a Nikon P150 camera with Nikkor 42× wide optical zoom lens.

2.2.5 Statistical analysis

Treatment across groups was randomly generated with animals coded by random identifiers. Investigators were blinded to treatment group during data acquisition and analysis. All values are expressed as the mean ± S.E.M. Comparison of data across all five experimental groups was performed by one-way analysis of variance (ANOVA). When the ANOVA indicated a significant difference between groups, comparison between each pair of groups was performed using Tukey's HSD test. *P*-values < 0.05 were considered statistically significant. Scatter plots show mean values with S.E.M. error bars.

3. Results

3.1 Phase I. EV characterization

3.1.1 Characterization of EPC-derived EVs

Enrichment of EVs from EPC culture media was confirmed by characterization of particle morphology and size distribution. TEM demonstrates the presence of small, round particles and cup-shaped particles between 60 and 120 nm characteristic of microvesicles and exosomes, respectively (*Figure 1A*). NTA on the EV isolate reveals that 80% of the sample falls within the range of 76.8–141.8 nm, with a modal particle diameter of 91.2 ± 2.9 nm (*Figure 1B*). EVs were isolated from serum-free EPC culture media to reduce serum protein and EV contamination. Serum-free conditions reduced EPC survival by 21.3% ($P < 0.01$) (see Supplementary material online, *Figure SIA*).

To compare EPCs and their released EVs, their proteomic profiles were investigated by mass spectrometry. Our analysis revealed more than 2000 unique proteins within EPCs and their EVs. Of these, 1327 were unique to EPCs, 47 were unique to EVs, and 662 were shared by both. Of note, the top 20 proteins most often found in exosomes, including the tetraspanins CD9, CD63, and CD81, were identified in our EV samples.[17,18] Several of the proteins shared between EPCs and EVs play important roles in angiogenesis, growth factors,[19–27] adhesion molecules,[28–33] enzymes and matrix proteins[24,34–37] (*Figure 1D*).

Low abundance proteins, including transcription factors, can escape detection by mass spectrometry. To account for this, analysis of protein interaction by MetaCore could infer the presence of 1770 additional interacting proteins not directly detected in the EPC and EV samples. Notably, c-Myc ($P = 2.2 \times 10^{-58}$) and Sp1 ($P = 4.5 \times 10^{-21}$), are inferred to be present with high probability (*Figure 1C*). Both c-Myc and Sp1 are known to play regulatory roles in the angiogenic pathway.[37–39]

3.1.2 EPC-derived EVs are uptaken by vascular endothelial cells through endocytosis

Uptake of EVs is essential to mediate their phenotypic effect. To confirm uptake of EPC-derived EVs, we visualized the uptake of CM-DiI-labelled EVs by HUVECs. After a 24-h incubation, confocal imaging showed clear, perinuclear staining of HUVECs with CM-DiI (*Figure 2A*). Most experimental evidence points to endocytosis as the primary mechanism of EV uptake.[40,41] To determine if endocytosis was responsible for EPC-derived EV uptake, CytoD, a known destabilizer of actin filaments was used to block uptake. As expected, we observed a dose-dependent decline in CM-DiI signal in HUVECs with CytoD preincubation (*Figure 2B–D*). On further quantification, there was an increase in CM-DiI signal intensity in the supernatant and complementary decrease in signal in the cells. (*Figure 2E* and *F*). These data suggest that endocytosis mediates the uptake of EPC-derived EVs into endothelial cells.

3.1.3 EV Treatment leads to increased organized vessel formation in vitro

Characterization of protein cargo present in EPC-derived EVs provides promising evidence of their potential to independently improve angiogenic activity in the same fashion as other progenitor cell therapies. To assess this, we performed a Matrigel tubule formation assay (*Figure 3*). Mean tubule length was significantly increased after incubation with EVs compared with EBM alone by 14.1% (157.9 ± 3.81 vs. 138.4 ± 2.92 units, *Figure 3D*). Incubation with EVs significantly reduced the number of isolated branches by 21% compared with EBM alone (47.5 ± 1.9 vs. 59.7 ± 1.3 branches, $P < 0.05$, *Figure 3e*), indicating an increase in overall organized vessel formation. We did not find a significant difference in HUVEC proliferation after incubation with EBM alone compared with incubation with EVs or VEGF (*Figure 3F*).

3.1.4 Steady release of EVs from STG

In our previous work with STG-encapsulated EPCs, we showed that the gel vehicle potentiated the effect of EPCs by minimizing cell dispersion.[14] We adapted this strategy to *in vivo* delivery of EVs to increase retention and local delivery of therapy via encapsulation within the STG (*Figure 4A*). The shear-thinning and viscoelastic behaviour of this gel was confirmed by oscillatory rheology (*Figure 4B*). Viscosity decreased with increasing shear rate and stress, displaying classical shear-thinning behavior. With increasing strain, gels yielded and the storage modulus (G') dropped below the loss modulus (G") to permit flow. Upon cessation of strain, gels rapidly recovered to initial mechanics in which G' predominates over G". CM-DiI EVs demonstrated even distribution without aggregation throughout the STG when imaged with confocal microscopy (*Figure 4C*). The releasate from the STG + EV construct was collected over 21 days *in vitro* and prepared for NTA in five fractions. Analysis showed steady cumulative particle release over 21 days (*Figure 4D*).

3.2 Phase II: EV treatment

3.2.1 STG + EPC and STG + EV treatments improve haemodynamics in a rat model of acute MI

After demonstrating the enhanced angiogenic potential of EPC-derived EVs *in vitro* and compatibility with the STG, we next sought to establish the impact of EVs in myocardial ischaemia. Four weeks after MI, rat hearts treated with STG + EV and STG + EPC showed improvements in haemodynamic function when compared to PBS Control and STG Control. The primary outcome of preload-independent contractility as measured by ESPVR was significantly higher in these groups compared

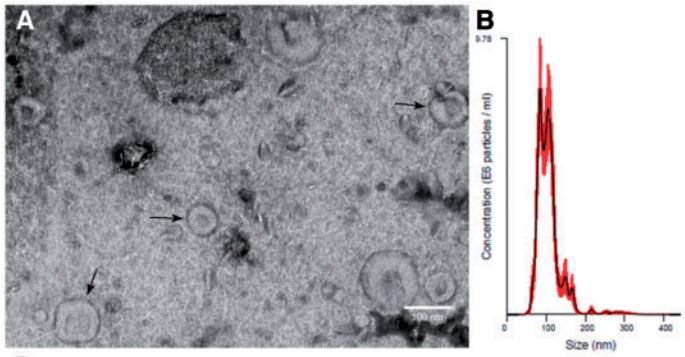

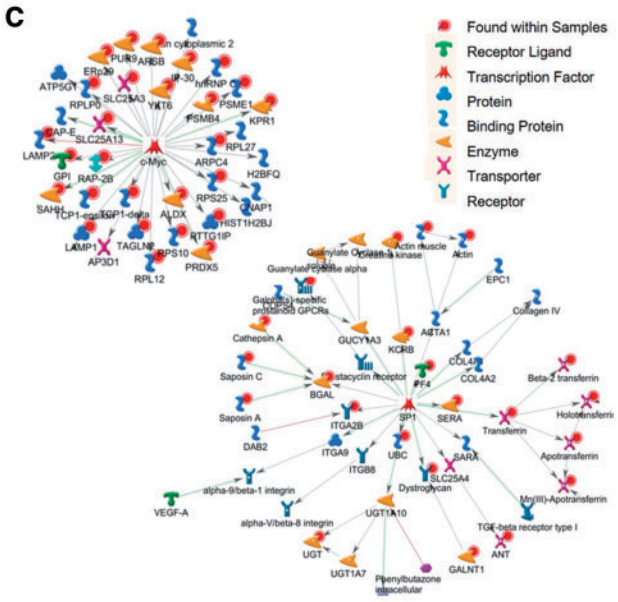

D

Exosome Markers[16,17]	CD9; PDCD6IP; HSPA8; GAPDH; ACTB; ANXA2; CD63; SDCBP; ENO1; HSP90AA1; TSG101; PKM; LDHA; EEF1A1; YWHAZ; PGK1; EEF2; ALDOA; HSP90AB1; ANXA5
Angiogenic Growth Factors[18–26]	ANPEP; NRP1; NRP2; TGFB1; STAB1; IGF1; ANXA2
Adhesion Molecules[27–32]	ITGAV; ITGB3; THBS1; FN1; ADAM15
Enzymes and Matrix Proteins[23,33–36]	PF4; MMP9; TIMP1; TIMP2; PLAU; GPX1
Transcription Factors[37]	HPSE

Figure 1 Characterization of EPC-derived EVs. (*A*) Representative TEM images of EV isolate show uniform 60–120 nm round particles. (*B*) NTA demonstrates characteristic size and distribution of EPC-derived EVs. Red shaded areas indicate S.E.M. (*C*) Network maps of interactions by proteins common to EPCs and EVs, and (*D*) characteristic exosome markers found in EVs and angiogenic proteins identified in both EPCs and EVs ($n = 3$).

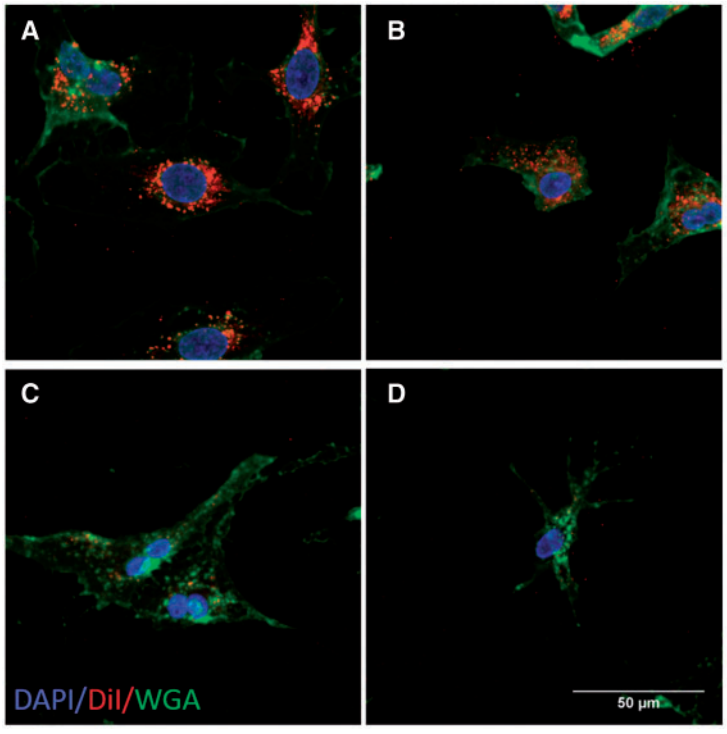

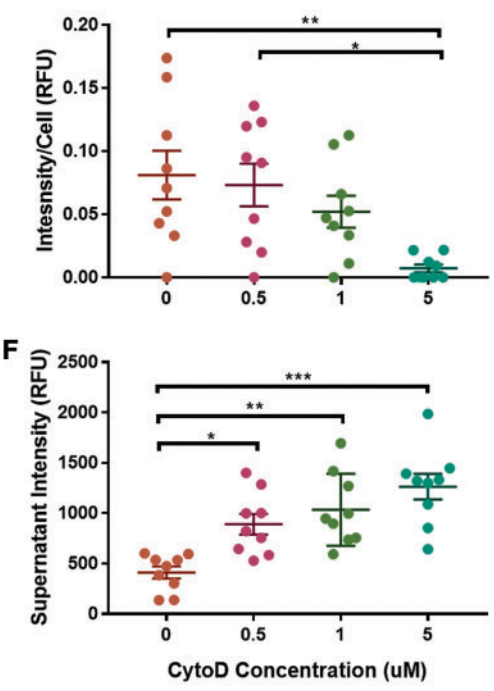

Figure 2 EV Uptake by HUVECs. (*A*) Confocal images taken at 63× show uptake of CM-DiI by perinuclear staining. Uptake was reduced after pre-incubation with CytoD at (*B*) 0.5 μM, (*C*) 1 μM, and (*D*) 5 μM. (*E*) CM-DiI signal intensity normalized to live cells. (*F*) CM-DiI signal intensity in the supernatant ($n = 9$, $^{*}P < 0.05$, $^{**}P < 0.01$, $^{***}P < 0.001$).

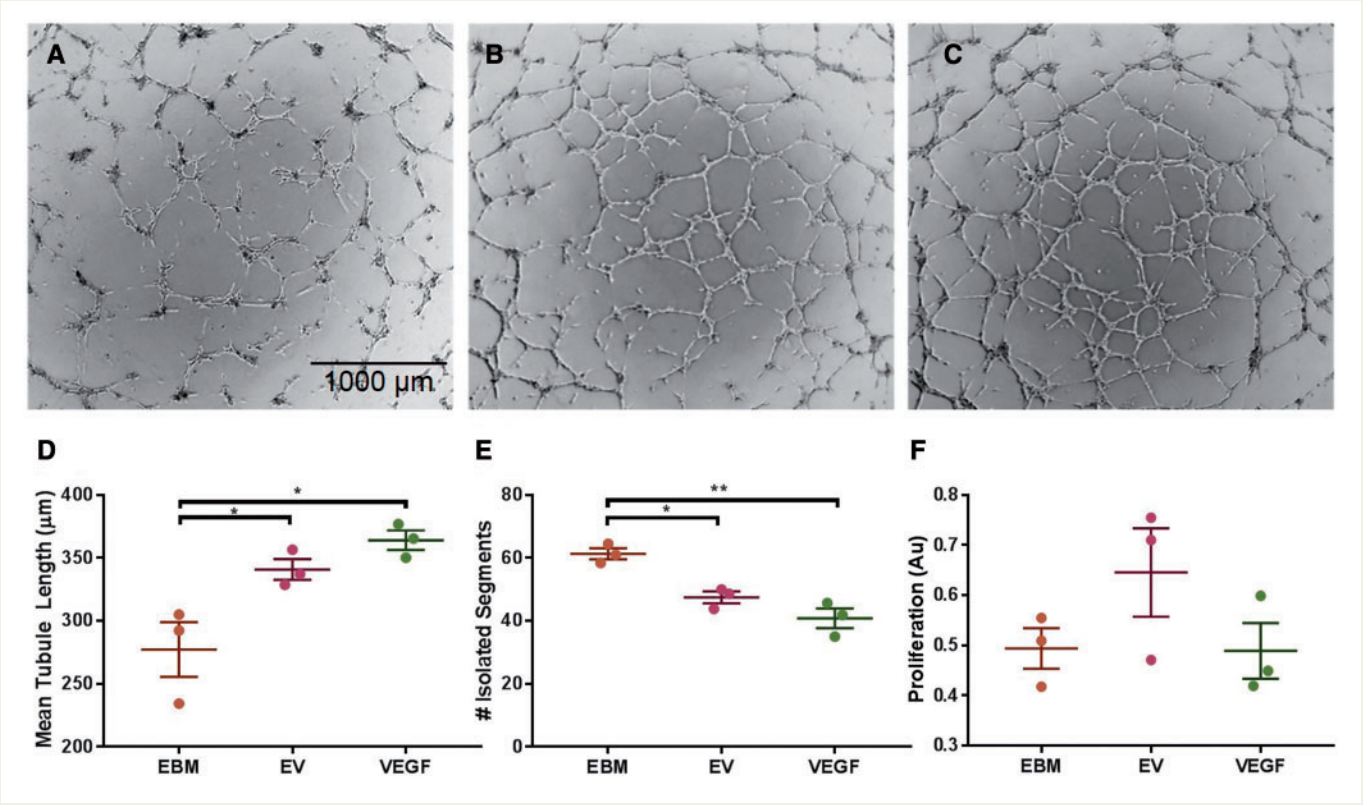

Figure 3 Tubule formation assay shows pro-angiogenic effect of EVs after 11 h. (*A*) HUVECs incubated in EBM alone, (*B*) with EVs, and (*C*) with 1 ng/ml VEGF. (*D*) Quantitative analysis of mean tubule length for each group. (*E*) Quantitative analysis of isolated segment, indicating disorganized tubule formation. (*F*) BrdU proliferation assay shows no significant difference in HUVEC proliferation after incubation with EBM alone, EVs, or VEGF ($n = 3$, $^{*}P < 0.05$, $^{**}P < 0.01$).

with controls (*Figure 5A*). ESPVR in the STG + EV cohort was 82% higher compared with PBS Control, 27% higher compared with STG Control, 16% higher compared with the PBS + EV group, and equivalent compared with STG + EPC (see Supplementary material online, *Figure SII*). When compared with PBS Control, STG + EV treatment increased left ventricular ejection fraction, cardiac output, maximum rate of systolic pressure change, maximum rate of diastolic pressure change, and maximum pressure (*Figure 5B–F*). These parameters were not statistically different between STG + EV and STG + EPC groups. When compared with PBS Control, STG + EV and STG + EPC animals had decreased end diastolic and systolic volumes but an overall increase in stroke volume (*Figure 5G–I*). In these groups, decreased left ventricular end diastolic volume provided evidence for the preservation of ventricular geometry. Furthermore, the STG + EV treatment also improved ventricular compliance, the reciprocal of EDPVR (*Figures 5J*). No significant trend was observed in heart rate among the treatment groups (*Figure 5K*).

3.2.2 STG + EV increases vessel density in peri-infarct myocardium

To better elucidate the mechanisms underlying the haemodynamic improvements observed by the STG + EV therapy, we assessed vascular density in the peri-infarct myocardium after treatment by looking at expression of vWF, expressed on the luminal side of vascular endothelial cells, and α- SMA, found in the smooth muscle lining arterioles. Overall, vascular density significantly improved in response to STG + EPC and STG + EV treatment (*Figure 6*). Of note, STG + EV showed significant improvement in microvascular density compared with STG alone (68.0 ± 3.2 vs. 46.4 ± 4.82 vessels/HPF, $P < 0.01$). This increase in microvascular density was observed for both capillary (48.5 ± 5.5 vs. 38.7 ± 4.8 vessels/HPF) and arteriolar (13.3 ± 1.8 vs. 7.8 ± 1.1 vessels/HPF) density. There was no significant change in vessel density between the PBS and PBS + EV groups (46.7 ± 4.5 vs. 42.3 ± 2.0 vessels/HPF). This may be a result of limited EV retention in the myocardium without STG encapsulation.

3.2.3 STG treatment alone increases recruitment of inflammatory cells

Quantification of CD11b expression in the ischaemic border zone after treatment with PBS Control, STG Control, and STG + EV showed increased inflammation in the STG Control and STG + EV groups compared with PBS Control 2 days after MI and treatment injection ($P < 0.05$). However, the addition of EVs to the treatment did not increase inflammatory cell recruitment from the baseline amount seen with injection of the empty STG. The increased border zone inflammation resolved by 4 weeks, and CD11b expression was no different in PBS Control compared with STG Control and STG + EV (*Figure 7*).

3.2.4 STG + EVs improves border zone remodeling post-infarction

Four weeks after LAD ligation and MI, all hearts demonstrated distinct areas of transmural infarct in addition to variable amounts of healthy

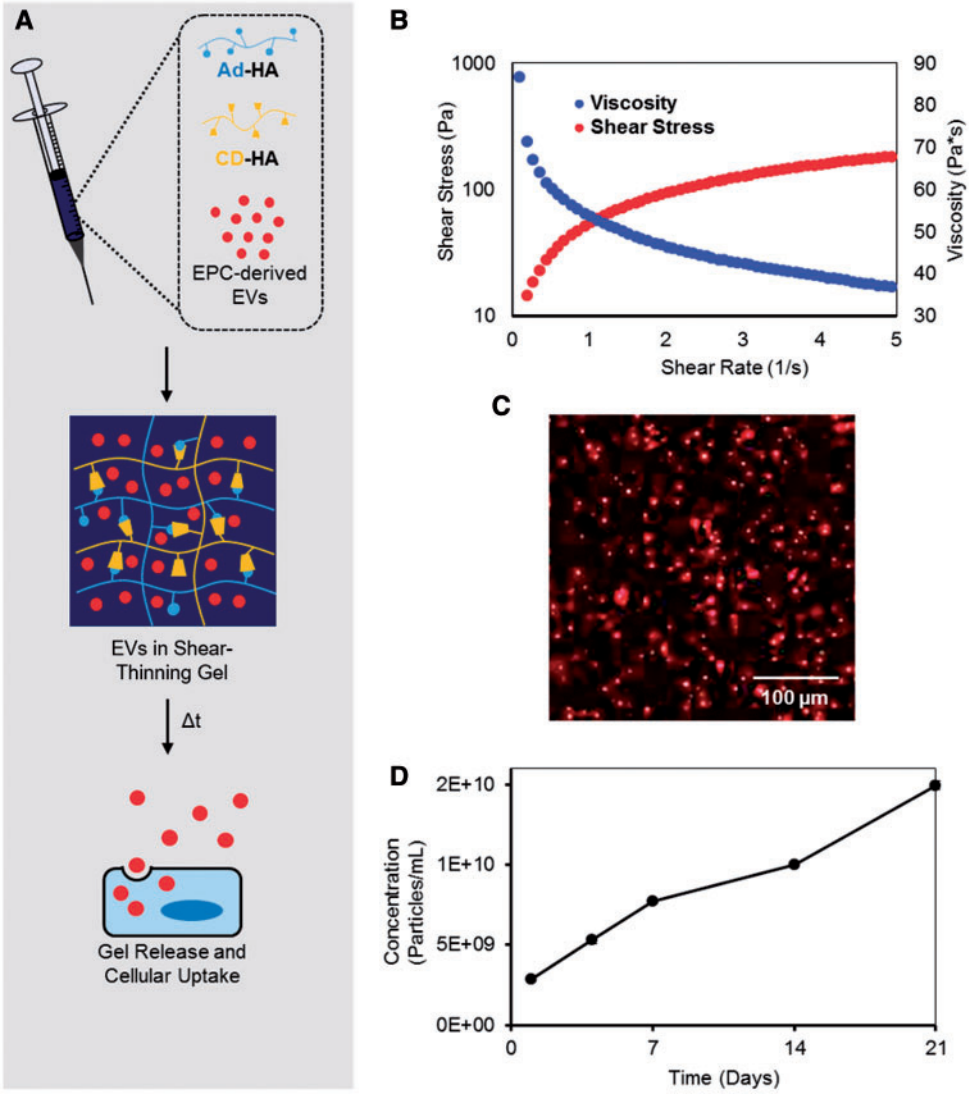

Figure 4 Steady release of EVs from STG. (*A*) EVs are added to CD-HA and Ad-HA and loaded into a syringe. CD-HA and Ad-HA interact through guest-host chemistry to form a supramolecular gel. (*B*) As the syringe plunger is depressed and shear stress is added, the gel shear-thins to permit flow as viscosity decreases with shear. Upon cessation of strain the gel rapidly recovers, re-assembling at the myocardial injection site with the EVs. (*C*) Confocal microscopy of CM-DiI-labelled EVs within the STG shows an even distribution. (*D*) EVs are released from the gel over time to permit cellular uptake. Cumulative EV release profile from the STG ($n = 2$) show steady particle release over 21 day. Error bars are hidden due to their relatively small magnitude.

myocardium intermingled with scar in the border zone. Scar thickness, as averaged across the scar's midpoint and border zone regions, was increased by 49% in STG + EV (10.8 ± 0.4 units) and 48% in STG + EPC (10.7 ± 0.3 units) compared with PBS Control (7.3 ± 0.6 units) (*Figure 8*). Scar thickness in the PBS + EV group (9.5 ± 0.4 units) was significantly improved from the PBS Control but not from STG Control. PBS and STG Control animals demonstrated no statistical significance in scar and border zone thickness.

4. Discussion

The purpose of this study was to advance the clinical translatability of angiogenic progenitor cell therapy through intramyocardial delivery of EVs within a gel, eliminating the obstacles associated with cell therapy. Using ESPVR as the primary measure of treatment effect, we demonstrated that paracrine factors alone can provide the same improvements in haemodynamic outcomes as progenitor cell therapy in the treatment of ischaemic myocardial insult.

This is the first known report of an injectable hydrogel system for sustained EV delivery in the myocardium. Starting with an isolation technique that reproducibly yielded an exosome-enriched fraction of EVs, we elucidated potential mechanisms of the observed positive haemodynamics effects via proteomic evidence of crucial therapeutic pathways and demonstration that EPC-derived EVs were taken up by resident endothelial cells to produce a robust angiogenic response. ESPVR increased 82% with STG + EV compared with PBS controls, whereas EV alone and STG alone produced a 56 and 43% increase in ESPVR compared with

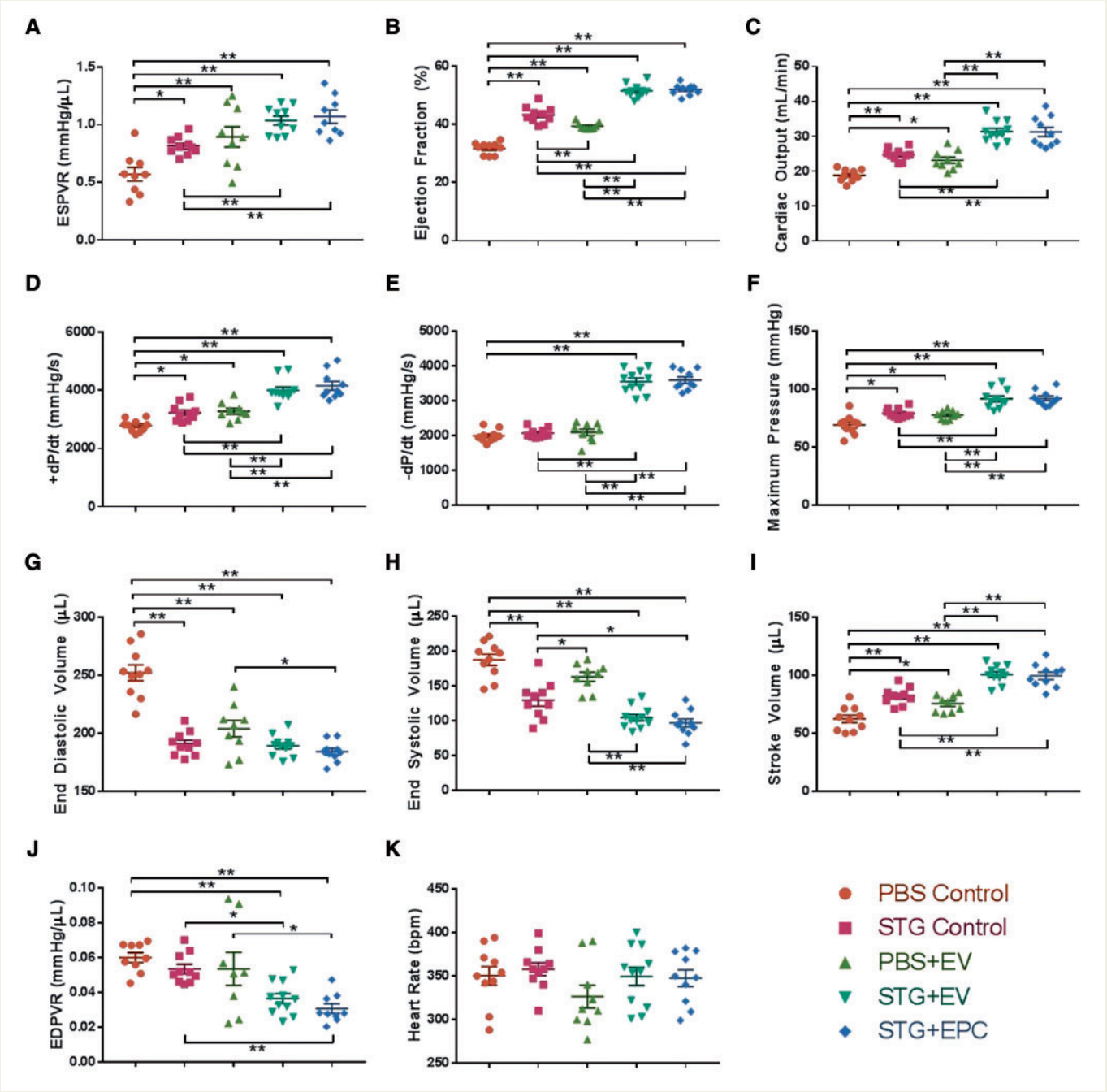

Figure 5 STG + EPC and STG + EV treatment improves haemodynamics in a rat model of acute MI. Left ventricular haemodynamic function measured by pressure-volume catheter of rat hearts 4 weeks after MI and untreated (PBS Control) or treated with combinations of the STG, EVs, or EPCs (*$P < 0.05$, **$P < 0.01$). Sample sizes were as follows: PBS Control, $n = 10$; STG Control, $n = 10$; PBS + EV, $n = 9$; STG + EV, $n = 11$; STG + EPC, $n = 10$. Abbreviations: ESPVR, end systolic pressure-volume relationship; +dP/dt, maximum change in systolic pressure over time; -dP/dt, maximum change in diastolic pressure over time; EDPVR, end-diastolic pressure–volume relationship.

PBS, respectively. It is thus clear that although each component had therapeutic potential when delivered as a standalone therapy, by delivering potent EVs by direct injection within a gel with controlled-release pharmacodynamic properties, the effect of the EVs was greatly potentiated. Secondary outcomes of peri-infarct vascular proliferation and myocardial scar thickness after MI were also enhanced with STG + EV treatment and were corroborated by proteomic analysis of EV content.

To parse out the various sources of treatment effect in this study, we saw a significant, though modest, improvement in ESPVR 4 weeks after LAD ligation and treatment injection comparing PBS Control and PBS + EV. This demonstrated a treatment effect of the isolated EVs alone.

The empty gel (STG Control) also conferred a significant advantage in ESPVR 4 weeks after MI compared with PBS Control. HA is a biologically active proangiogenic molecule, exerting effects on endothelial cell

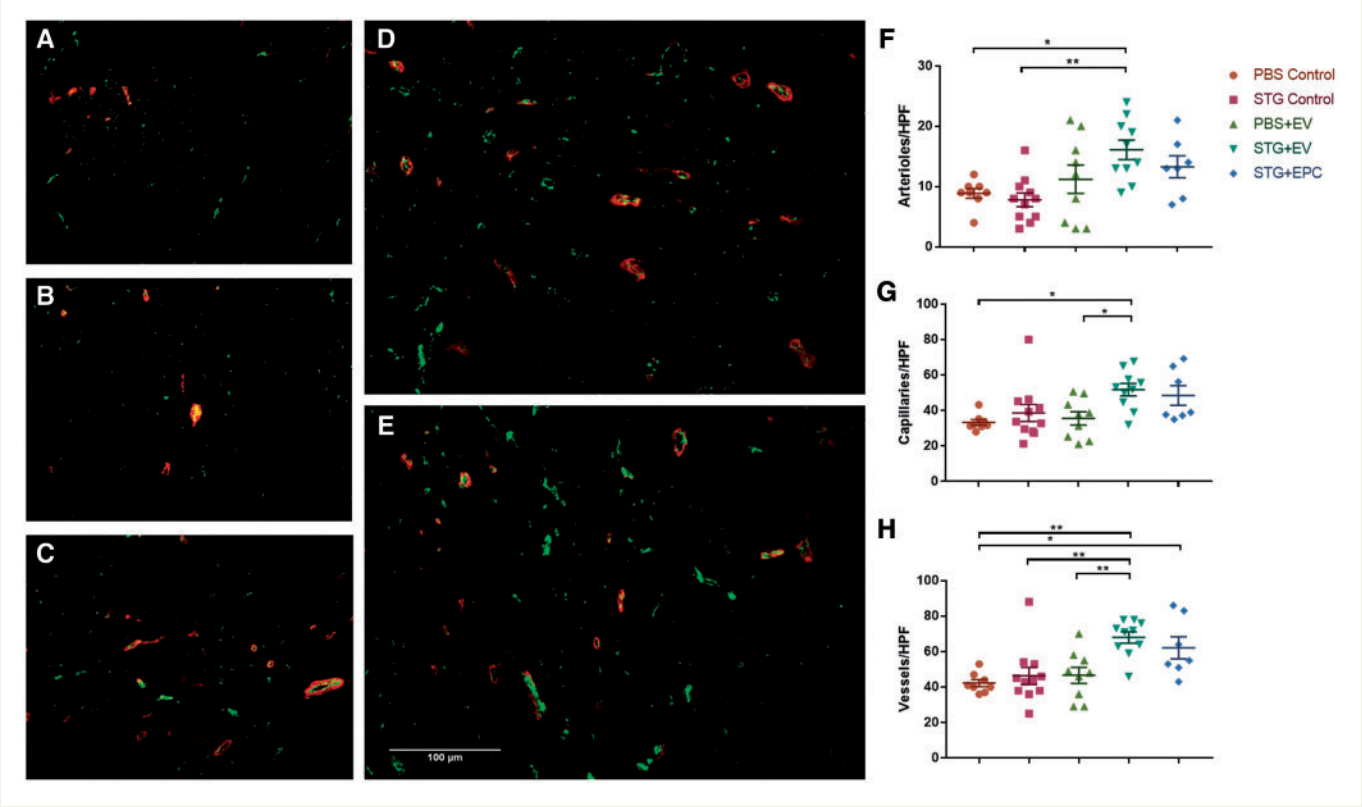

Figure 6 STG + EV increases vessel density in peri-infarct myocardium. immunohistochemistry at 20× magnification of peri-infarct myocardium to quantify vascular density in hearts treated with (*A*) PBS Control, (*B*) STG Control, (*C*) PBS + EV, (*D*) STG + EV, and (*E*) STG + EPC. Blue, DAPI; green, vWF; red, SAM. Quantification of the mean number of (*F*) arterioles (*G*) capillaries (*H*) and total vessels per HPF. Sample sizes were as follows: PBS Control, $n = 8$; STG Control, $n = 11$; PBS+ EV, $n = 9$; STG + EPC, $n = 7$, STG + EV, $n = 10$ (*$P < 0.05$, **$P < 0.01$).

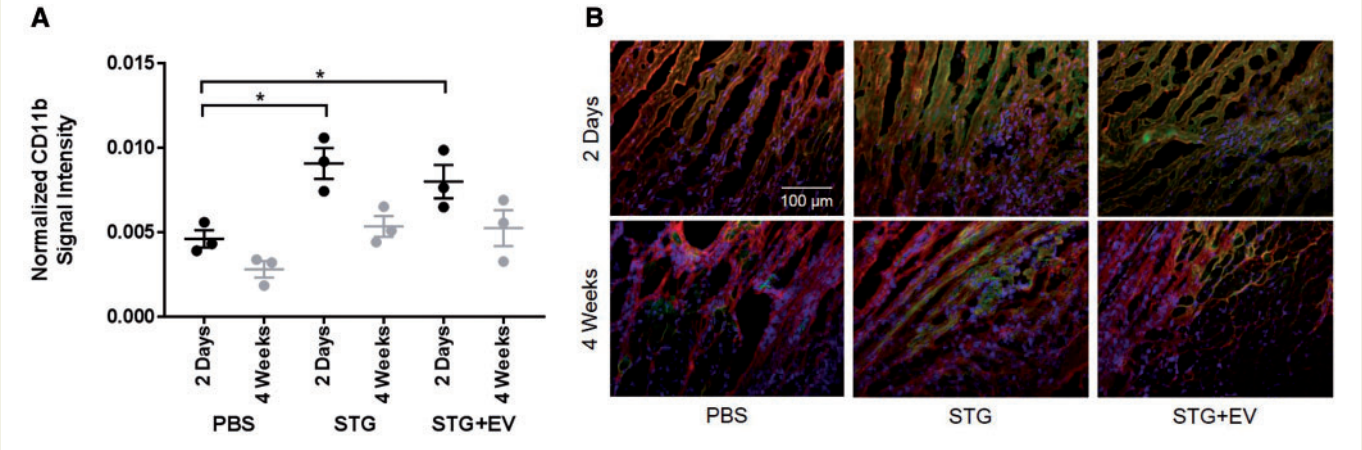

Figure 7 Normalized CD11b signal intensity. (*A*) Quantification of inflammatory cell infiltration into the ischaemic border zone after treatment with PBS Control, STG Control, and STG + EV showed increased inflammation in the STG and STG + EV groups compared with PBS Control 2 days after MI and treatment injection (black data points, $n = 3$, *$P < 0.05$). The addition of EVs to the treatment did not increase inflammatory cell recruitment from the baseline amount after the injection of the empty STG. At 4 weeks, the inflammation in the STG Control and STG + EV groups was no different from that in the PBS Control group (grey data points, $n = 3$). (*B*) Representative images of the ischaemic border zone at 2 days and 4 weeks. Blue, DAPI; green, CD11b; red, WGA.

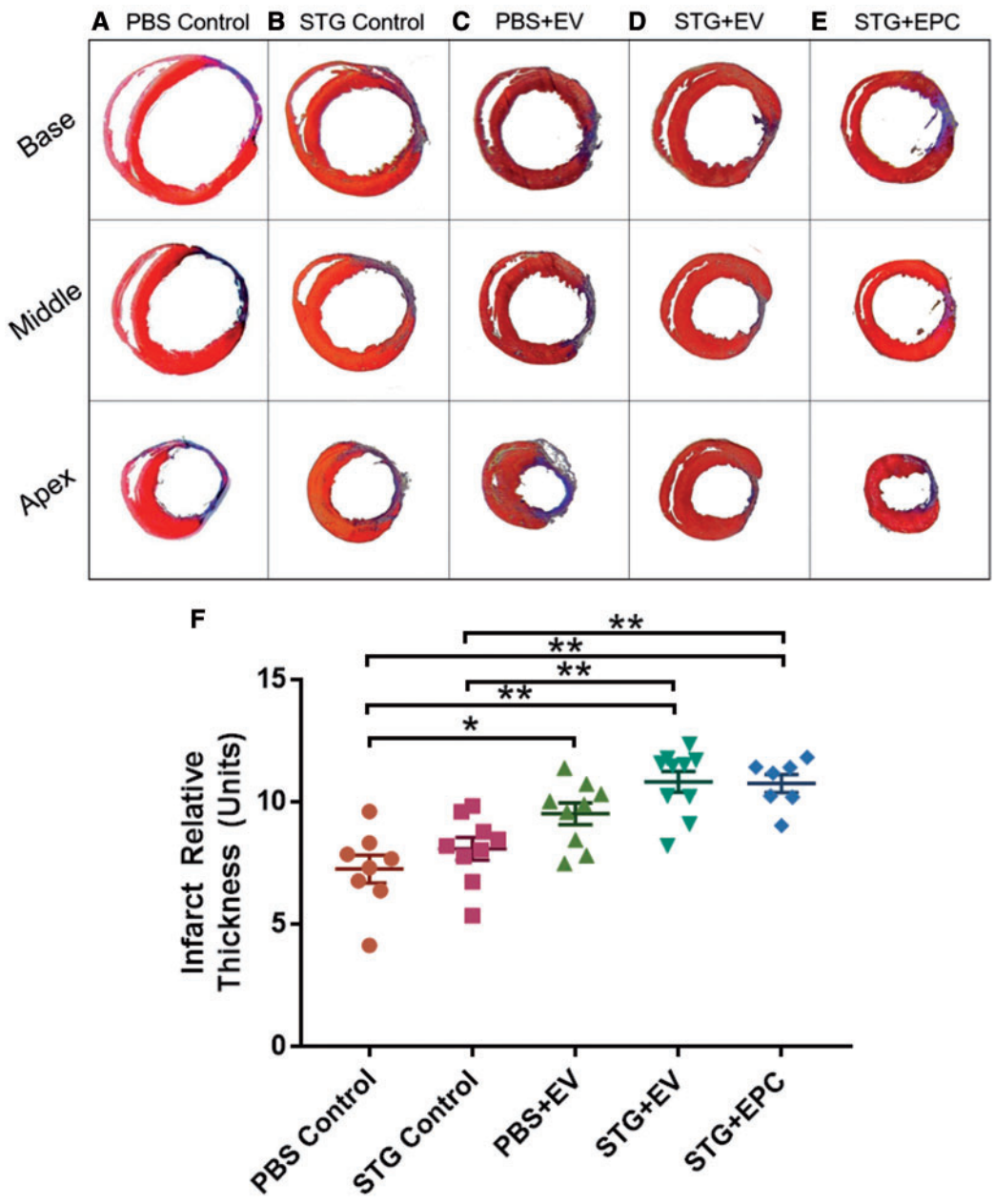

Figure 8 STG + EVs improve border zone remodelling post-infarction. representative images of sections taken at the upper, middle, and lower scar 4 weeks after infarct for (*A*) PBS Control, (*B*) STG Control, (*C*) PBS + EV, (*D*) STG + EV, and (*E*) STG + EPC where viable muscle is stained red, and collagen scar is stained blue. (*F*) Quantified scar thickness for all groups. Sample sizes were as follows: PBS Control, $n = 8$; STG Control, $n = 9$; PBS + EV, $n = 9$; STG + EV, $n = 10$; STG + EPC, $n = 7$ (*$P < 0.05$, **$P < 0.01$).

proliferation, migration, and tubule formation through CD44 and receptor for HA-mediated cell motility signalling.[42] Furthermore, the stiffness of the STG may serve to mechanically stabilize the infarct border zone and reduce stress in this region.[43] In line with previous studies of HA-based hydrogels,[44] we detected an early increase in inflammation in the ischaemic border zone after injection of the STG that was not modified by the addition of EVs to the STG. This inflammation may aid in early infarct remodelling and had resolved by 4 weeks after MI.

Our data suggest that a dynamic interaction existed between EVs and STG with the STG + EV therapy having significant advantages over STG Control in ESPVR. Similarly, the STG + EV treatment was significantly more effective than PBS + EV, likely owing to the sustained release of EVs from the STG and the resulting prolonged exposure of the border zone myocardium to EVs in the STG + EV group compared with the PBS + EV group. Extrapolating from experiences with cell-based therapy, it is likely that the small size of EVs resulted in rapid washout from the myocardium soon after injection when delivered in PBS.

Finally, we found that STG + EV and STG + EPC were equivalent in the treatment of ischaemic myocardium when judged by our defined

endpoints. Although STG allowed the sustained release of the EVs over an extended period of time, EPCs were likely also producing EVs that were slowly released into the myocardium. These *in vivo* measures, along with the proteomic overlap between EVs and EPCs, convincingly demonstrated that EVs alone were sufficient to produce similar therapeutic benefits to the EPCs from which they were derived. However, EVs—especially the sizable exosome component—provided important advantages over cell-based therapy.

Our study corroborates the results of numerous previous studies that have shown a correlation between increased peri-infarct angiogenesis and improved haemodynamic function.[45] Improving the supply of oxygen- and nutrient-rich blood to the peri-infarct cardiomyocytes led to preserved contractility, while cardiomyocytes in the infarct border zone underwent hibernation with resultant contractile dysfunction in the setting of chronic ischaemia.[46] Functional outcomes were further supported by histologic analyses revealing significantly thicker scars in our therapeutic treatment groups. Our measurement of scar thickness reflected the thickness of the border zone, as thickness was calculated by averaging the scar midpoint and the peripheral scar/border zone region located on either end. Increased angiogenesis in the border zone of treated hearts likely improved local cardiomyocyte recovery and decreased adverse ventricular remodelling in the peri-infarct region, thereby minimizing thinning of infarcts and preserving global ventricular geometry. As a result, the end diastolic volume was significantly lower in STG + EV and STG + EPC animals compared with PBS Control. Given the progressive dilation of the heart after infarct with asymmetric expansion of the remote myocardium compared with the collagen scar, we found scar length to be unreliable as its measurement was confounded by the presumed treatment effect.

There are several limitations to this study. Although ultracentrifugation and polymer-based precipitation methods are efficient and widely used methods of EV isolation, these methods did not completely eliminate non-EV material from the CM isolate. Furthermore, the quantification of *in vitro* angiogenesis under normoxic conditions in our study did not fully mirror the *in vivo* model in which the EVs were injected into an acutely ischaemic myocardium. However, given the complex compensatory mechanisms which were stimulated *in vivo* in the face of an ischaemic insult, simply performing *in vitro* angiogenesis assays in hypoxic environments was unlikely to fully capture the true effect of ischaemia within an animal model. To improve the mechanistic understanding of EV induced angiogenesis, a 3D angiogenesis assay such as the *in vivo* Matrigel plug assay in ischaemic tissue may be of interest.

This study has established significant foundational knowledge regarding the therapeutic value of EPC-derived EVs, but to understand the full potential of this treatment, many future projects remain. An exciting avenue for future development of EV therapy revolves around a better understanding of how environmental conditions can be manipulated to alter the essential cargo packaged within EVs. Furthermore, the benefits of using STG as a vehicle for EV delivery could be translated to the clinical setting via percutaneous catheter injections after acute MI, and large animal studies are needed to scale and trial this approach. Further detailed investigation into the immunogenicity of EVs will inform the therapeutic strategy for EV use in large animals, and eventual clinical human applications.

Supplementary material

Supplementary material is available at *Cardiovascular Research* online.

Acknowledgements

The authors would like to thank Rahul Kanade, Alexander Zhou, Murray Skolnik, Elizabeth Li, and Rohith Thaiparambil for their assistance with data acquisition and analysis and Matthew Haney from the University of North Carolina Nanomedicines Characterization Core Facility for his expertise with nanoparticle tracking analysis.

Conflict of interest: none declared.

Funding

This study was supported by the American Heart Association through a Scientist Development Grant (SDG 17230005 to P.A.), predoctoral fellowship (to L.L.W.), and an Established Investigator Award (to J.A.B.). The study was also supported by the National Institutes of Health (R01 HL135090 to P.A., F30 HL134255 to L.L.W., and R01 HL107938 and R01 HL063954 to J.A.B.).

References

1. Murphy SL, Xu J, Kochanek KD. Deaths: final data for 2010. *Natl Vital Stat Rep* 2013;**61**:1–117.
2. Head SJ, Mack MJ, Holmes DR, Jr, Mohr FW, Morice MC, Serruys PW, Kappetein AP. Incidence, predictors and outcomes of incomplete revascularization after percutaneous coronary intervention and coronary artery bypass grafting: a subgroup analysis of 3-year SYNTAX data. *Eur J Cardiothorac Surg* 2012;**41**:535–541.
3. Sutton MG, Sharpe N. Left ventricular remodeling after myocardial infarction: pathophysiology and therapy. *Circulation* 2000;**101**:2981–2988.
4. Sheikh AY, Huber BC, Narsinh KH, Spin JM, van der Bogt K, de Almeida PE, Ransohoff KJ, Kraft DL, Fajardo G, Ardigo D, Ransohoff J, Bernstein D, Fischbein MP, Robbins RC, Wu JC. In vivo functional and transcriptional profiling of bone marrow stem cells after transplantation into ischemic myocardium. *Arterioscler Thromb Vasc Biol* 2012;**32**:92–102.
5. Li SH, Lai TY, Sun Z, Han M, Moriyama E, Wilson B, Fazel S, Weisel RD, Yau T, Wu JC, Li RK. Tracking cardiac engraftment and distribution of implanted bone marrow cells: comparing intra-aortic, intravenous, and intramyocardial delivery. *J Thorac Cardiovasc Surg* 2009;**137**:1225–1233.e1.
6. Gnecchi M, He H, Liang OD, Melo LG, Morello F, Mu H, Noiseux N, Zhang L, Pratt RE, Ingwall JS, Dzau VJ. Paracrine action accounts for marked protection of ischemic heart by Akt-modified mesenchymal stem cells. *Nat Med* 2005; **11**:367–368.
7. Sahoo S, Klychko E, Thorne T, Misener S, Schultz KM, Millay M, Ito A, Liu T, Kamide C, Agrawal H, Perlman H, Qin G, Kishore R, Losordo DW. Exosomes from human CD34+ stem cells mediate their proangiogenic paracrine activity. *Circ Res* 2011;**109**:724–728.
8. Ibrahim AGE, Cheng K, Marbán E. Exosomes as critical agents of cardiac regeneration triggered by cell therapy. *Stem Cell Rep* 2014;**2**:606–619.
9. Bussche L, Rauner G, Antonyak M, Syracuse B, McDowell M, Brown AM, Cerione RA, Van de Walle GR. Microvesicle-Mediated Wnt/β-catenin signaling promotes interspecies mammary stem/progenitor cell growth. *J Biol Chem* 2016;**291**:24390–24405.
10. El Andaloussi S, Mäger I, Breakefield XO, Wood MJ. Extracellular vesicles: biology and emerging therapeutic opportunities. *Nat Rev Drug Discov* 2013;**12**:347–357.
11. Ibrahim A, Marbán E. Exosomes: Fundamental Biology and Roles in Cardiovascular Physiology. *Annu Rev Physiol* 2016; **78**:67–83.
12. Valadi H, Ekström K, Bossios A, Sjöstrand M, Lee JJ, Lötvall JO. Exosome-mediated transfer of mRNAs and microRNAs is a novel mechanism of genetic exchange between cells. *Nat Cell Biol* 2007;**9**:654–659.
13. Sokolova V, Ludwig AK, Hornung S, Rotan O, Horn PA, Epple M, Giebel B. Characterisation of exosomes derived from human cells by nanoparticle tracking analysis and scanning electron microscopy. *Colloids Surf B Biointerfaces* 2011;**87**:146–150.
14. Gaffey AC, Chen MH, Venkataraman CM, Trubelja A, Rodell CB, Dinh PV, Hung G, MacArthur JW, Soopan RV, Burdick JA, Atluri P. Injectable shear-thinning hydrogels used to deliver endothelial progenitor cells, enhance cell engraftment, and improve ischemic myocardium. *J Thorac Cardiovasc Surg* 2015;**150**:1268–1277.
15. Atluri P, Miller JS, Emery RJ, Hung G, Trubelja A, Cohen JE, Lloyd K, Han J, Gaffey AC, MacArthur JW, Chen CS, Woo YJ. Tissue-engineered, hydrogel-based endothelial progenitor cell therapy robustly revascularizes ischemic myocardium and preserves ventricular function. *J Thorac Cardiovasc Surg* 2014;**148**:1090–1098.
16. Pacher P, Nagayama T, Mukhopadhyay P, Bátkai S, Kass DA. Measurement of cardiac function using pressure-volume conductance catheter technique in mice and rats. *Nat Protoc* 2008;**3**:1422–1434.
17. Keerthikumar S, Chisanga D, Ariyaratne D, Al Saffar H, Anand S, Zhao K, Samuel M, Pathan M, Jois M, Chilamkurti N, Gangoda L, Mathivanan S. ExoCarta: a web-based compendium of exosomal cargo. *J Mol Biol* 2016;**428**:688–692.

18. Mathivanan S, Fahner CJ, Reid GE, Simpson RJ. ExoCarta 2012: database of exosomal proteins, RNA and lipids. *Nucleic Acids Res* 2012;**40**:D1241–D1244.
19. Dondossola E, Corti A, Sidman RL, Arap W, Pasqualini R. Bone marrow-derived CD13 cells sustain tumor progression: a potential non-malignant target for anti-cancer therapy. *OncoImmunology* 2014;**3**:e27716.
20. Rangel R, Sun Y, Guzman-Rojas L, Ozawa MG, Sun J, Giordano RJ, Van Pelt CS, Tinkey PT, Behringer RR, Sidman RL, Arap W, Pasqualini R. Impaired angiogenesis in aminopeptidase N-null mice. *Proc Natl Acad Sci USA* 2007;**104**:4588–4593.
21. Guzman-Rojas L, Rangel R, Salameh A, Edwards JK, Dondossola E, Kim Y-G, Saghatelian A, Giordano RJ, Kolonin MG, Staquicini FI, Koivunen E, Sidman RL, Arap W, Pasqualini R. Cooperative effects of aminopeptidase N (CD13) expressed by nonmalignant and cancer cells within the tumor microenvironment. *Proc Natl Acad Sci USA* 2012;**109**:1637–1642.
22. Raimondi C, Brash JT, Fantin A, Ruhrberg C. NRP1 function and targeting in neurovascular development and eye disease. *Prog Retin Eye Res* 2016;**52**:64–83.
23. Ling Q, Jacovina AT, Deora A, Febbraio M, Simantov R, Silverstein RL, Hempstead B, Mark WH, Hajjar KA. Annexin II regulates fibrin homeostasis and neoangiogenesis in vivo. *J Clin Invest* 2004;**113**:38–48.
24. Yan M, Lesyk G, Radziwon-Balicka A, Jurasz P. Pharmacological regulation of platelet factors that influence tumor angiogenesis. *Semin Oncol* 2014;**41**:370–377.
25. Pickup M, Novitskiy S, Moses HL. The roles of TGFβ in the tumour microenvironment. *Nat Rev Cancer* 2013;**13**:788–799.
26. Haider HK, Jiang S, Idris NM, Ashraf M. IGF-1-overexpressing mesenchymal stem cells accelerate bone marrow stem cell mobilization via paracrine activation of SDF-1α/CXCR4 signaling to promote myocardial repair. *Circ Res* 2008;**103**:1300–1308.
27. Kzhyshkowska J, Workman G, Cardó-Vila M, Arap W, Pasqualini R, Gratchev A, Krusell L, Goerdt S, Sage EH. Novel function of alternatively activated macrophages: stabilin-1-mediated clearance of SPARC. *J Immunol* 2006;**176**:5825–5832.
28. Avraamides CJ, Garmy-Susini B, Varner JA. Integrins in angiogenesis and lymphangiogenesis. *Nat Rev Cancer* 2008;**8**:604–617.
29. Cayrol F, Diaz Flaque MC, Fernando T, Yang SN, Sterle HA, Bolontrade M, Amoros M, Isse B, Farias RN, Ahn H, Tian YF, Tabbo F, Singh A, Inghirami G, Cerchietti L, Cremaschi GA. Integrin αvβ3 acting as membrane receptor for thyroid hormones mediates angiogenesis in malignant T cells. *Blood* 2015;**125**:841–851.
30. Lawler PR, Lawler J. Molecular basis for the regulation of angiogenesis by thrombospondin-1 and -2. *Cold Spring Harb Perspect Med* 2012;**2**:a006627.
31. Wang X, Hu Q, Nakamura Y, Lee J, Zhang G, From AH, Zhang J. The role of the sca-1+/CD31- cardiac progenitor cell population in postinfarction left ventricular remodeling. *Stem Cells* 2006;**24**:1779–1788.
32. Kim S, Bell K, Mousa SA, Varner JA. Regulation of angiogenesis in vivo by ligation of integrin alpha5beta1 with the central cell-binding domain of fibronectin. *Am J Pathol* 2000;**156**:1345–1362.
33. Horiuchi K, Weskamp G, Lum L, Hammes H-P, Cai H, Brodie TA, Ludwig T, Chiusaroli R, Baron R, Preissner KT, Manova K, Blobel CP. Potential role for ADAM15 in pathological neovascularization in mice. *Mol Cell Biol* 2003;**23**:5614–5624.
34. Pepper MS. Role of the matrix metalloproteinase and plasminogen activator-plasmin systems in angiogenesis. *Arterioscler Thromb Vasc Biol* 2001;**21**:1104–1117.
35. Yabluchanskiy A, Ma Y, Iyer RP, Hall ME, Lindsey ML. Matrix metalloproteinase-9: many shades of function in cardiovascular disease. *Physiol* 2013;**28**:391–403.
36. Moses MA. The regulation of neovascularization of matrix metalloproteinases and their inhibitors. *Stem Cells* 1997;**15**:180–189.
37. Galasso G, Schiekofer S, Sato K, Shibata R, Handy DE, Ouchi N, Leopold JA, Loscalzo J, Walsh K. Impaired angiogenesis in glutathione peroxidase-1-deficient mice is associated with endothelial progenitor cell dysfunction. *Circ Res* 2006;**98**:254–261.
38. He C, Hu H, Braren R, Fong SY, Trumpp A, Carlson TR, Wang RA. C-myc in the hematopoietic lineage is crucial for its angiogenic function in the mouse embryo. *Development* 2008;**135**:2467–2477.
39. Liu N, Ding D, Hao W, Yang F, Wu X, Wang M, Xu X, Ju Z, Liu J-P, Song Z, Shay JW, Guo Y, Cong Y-S. hTERT promotes tumor angiogenesis by activating VEGF via interactions with the Sp1 transcription factor. *Nucleic Acids Res* 2016;**44**:8693–8703.
40. Morelli AE, Larregina AT, Shufesky WJ, Sullivan MLG, Stolz DB, Papworth GD, Zahorchak AF, Logar AJ, Wang Z, Watkins SC, Falo LD, Thomson AW. Endocytosis, intracellular sorting, and processing of exosomes by dendritic cells. *Blood* 2004;**104**:3257–3266.
41. Mulcahy LA, Pink RC, Carter DR. Routes and mechanisms of extracellular vesicle uptake. *J Extracell Vesicles* 2014;**3**:24641.
42. Park D, Kim Y, Kim H, Kim K, Lee Y-S, Choe J, Hahn J-H, Lee H, Jeon J, Choi C, Kim Y-M, Jeoung D. Hyaluronic acid promotes angiogenesis by inducing RHAMM-TGFβ receptor interaction via CD44-PKCδ. *Mol Cells* 2012;**33**:563–574.
43. Ifkovits JL, Tous E, Minakawa M, Morita M, Robb JD, Koomalsingh KJ, Gorman JH, Gorman RC, Burdick JA. Injectable hydrogel properties influence infarct expansion and extent of postinfarction left ventricular remodeling in an ovine model. *Proc Natl Acad Sci USA* 2010;**107**:11507–11512.
44. Tous E, Ifkovits JL, Koomalsingh KJ, Shuto T, Soeda T, Kondo N, Gorman JH, Gorman RC, Burdick JA. Influence of injectable hyaluronic acid hydrogel degradation behavior on infarction-induced ventricular remodeling. *Biomacromolecules* 2011;**12**:4127–4135.
45. Orlic D, Kajstura J, Chimenti S, Limana F, Jakoniuk I, Quaini F, Nadal-Ginard B, Bodine DM, Leri A, Anversa P. Mobilized bone marrow cells repair the infarcted heart, improving function and survival. *Proc Natl Acad Sci USA* 2001;**98**:10344–10349.
46. Schinkel AFL, Bax JJ, Delgado V, Poldermans D, Rahimtoola SH. Clinical relevance of hibernating myocardium in ischemic left ventricular dysfunction. *Am J Med* 2010;**123**:978–986.